

## Article

# Investigating the Amenability of a PGM-Bearing Ore to Coarse Particle Flotation

Jestos Taguta, Mehdi Safari \*, Veruska Govender and Deshenthree Chetty

Mintek, 200 Malibongwe Drive, Randburg, Johannesburg 2194, South Africa

\* Correspondence: mehdis@mintek.co.za

**Abstract:** Coarse particle flotation (CPF) is one of the strategies employed to reduce energy consumption in mineral-processing circuits. Hydrofloat™ (HF) technology has been successfully applied in the coarse flotation of industrial minerals and sulphide middlings. However, this technology has not yet been applied in platinum group minerals (PGMs) flotation. In this paper, the amenability of platinum group minerals to CPF was investigated. Extensive flotation testwork was conducted to optimise the hydrodynamic parameters, i.e., bed level, air and water flow rates, in the flotation of coarse PGM feed using Hydrofloat. Mineralogical analysis of the feed and selected flotation products was conducted to understand the reasons for the recovery and loss of the valuable minerals. The results showed that the HF separator could upgrade the PGM ore with particles as coarse as +106 – 300 µm. For the optimised test, a reasonable Pt, Pd and Au recovery of 84% was achieved at a grade of 10 g/t and 16.5% mass pull, despite the platinum group minerals being poorly liberated (4.5 vol% fully liberated). The results demonstrated that HF achieved high recovery efficiencies across the 150–300 microns size fraction. The HF was therefore able to substantially increase the upper particle size that can be successfully treated by flotation in PGM operations. It was found that an increase in bed height, water rate and air flow rate resulted in an increase in recovery to a maximum. A further increase in the hydrodynamic parameters resulted in a decline in recovery. Hydrofloat outperformed the conventional Denver flotation machine across the following size fractions: +106 – 150 µm, +150 – 212 µm, +212 – 250 µm and +250 – 300 µm. The practical implications of the findings on the modification of existing circuits and the design of novel flowsheets for the processing of PGM ores with less water and energy consumption are discussed.



**Citation:** Taguta, J.; Safari, M.; Govender, V.; Chetty, D. Investigating the Amenability of a PGM-Bearing Ore to Coarse Particle Flotation. *Minerals* **2023**, *13*, 698. <https://doi.org/10.3390/min13050698>

Academic Editors: Feridun Boylu, Orhan Özdemir and Onur Guven

Received: 23 April 2023

Revised: 7 May 2023

Accepted: 18 May 2023

Published: 20 May 2023



**Copyright:** © 2023 by the authors. Licensee MDPI, Basel, Switzerland. This article is an open access article distributed under the terms and conditions of the Creative Commons Attribution (CC BY) license (<https://creativecommons.org/licenses/by/4.0/>).

**Keywords:** coarse particle flotation; Hydrofloat™ technology; mineralogy; platinum group minerals

## 1. Introduction

South Africa supplies almost 80% of the world's platinum group elements (PGE) demands, contributing significantly to the economy of the country because of a massive resource deposit called the Bushveld Complex, BC [1,2]. The PGEs are extracted from three mineralised horizons, namely the Merensky, UG-2 and Plat reefs. The flotation efficiency of platinum group minerals (PGM) ores using conventional mechanical cells is hugely dependent on liberation. Conventional comminution circuits, comprising a cone crusher, high-pressure grinding roll (HPGR) and ball mill, targeting a primary grind of 80% passing 75 µm, are energy-intensive, as the finer the product size, the higher the energy consumption rate [3–5]. Fine grinding leads to the sliming of PGMs and BMS (base metal sulphides) due to overgrinding, thereby resulting in losses. Some PGM operations implement staged grinding utilising a complex mill, float, mill, float (MF2) circuit, as shown in Figure 1, in order to prevent overgrinding. A number of PGM concentrators implement flash flotation to recover coarse liberated PGMs and BMS in the hydrocyclone underflow stream, before recycling them back to the mill.

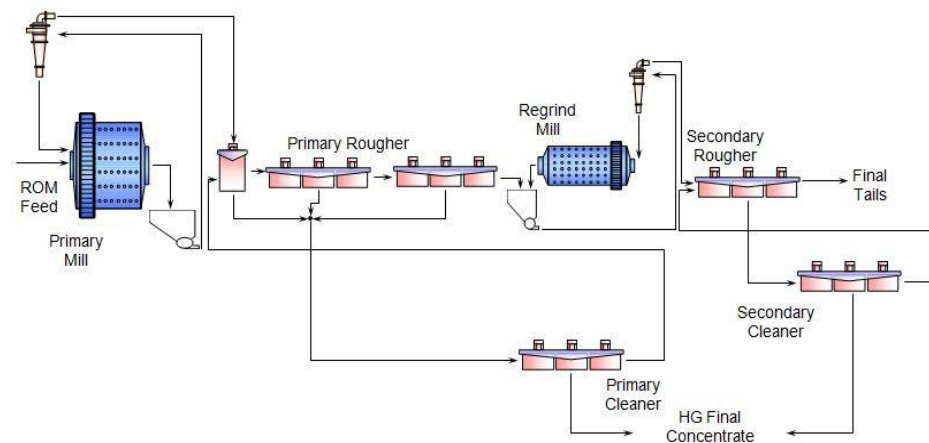


**Figure 1.** Typical MF2 flotation flowsheets used for the processing of Platreef ores.

Apart from the high energy consumption, finer grinding also generates fines, which are difficult to recover using conventional mechanical flotation cells [6–9]. Conventional sulphide flotation machines are typically limited to a particle size range of 10–100  $\mu\text{m}$  due to inherent constraints created by the pulp and froth phases [10]. This phenomenon is depicted in the well-recognised “elephant curve” [11].

The decline in the recovery of coarse particles (>100  $\mu\text{m}$ ) is attributed to many reasons, including poor liberation [12–14], the low carrying capacity of bubbles [15,16], and the detachment of bubble-particle aggregates due to high turbulence [17–20]. The poor recovery of fines (<10  $\mu\text{m}$ ) is attributed to low collision efficiencies with relatively large bubbles [21,22]. The fines are slow-floating and thus require longer residence times, high turbulence, and relatively higher collector dosages due to high particle surface area. Increasing turbulence comes at the cost of higher energy consumption. In a cost breakdown study of large flotation cells, it was established that approximately 68% of the total operating cost is attributed to energy consumption [23].

The inherent limitations associated with the conventional flotation machines to recover coarse particles can be overcome by new technologies such as Eriez’s Hydrofloat™, a fluidised-bed (teeter-bed) separator which synergistically combines flotation and gravity separation for the selective recovery of feeds containing very coarse particles [24]. The lab scale Hydrofloat (HF) separator used in this study is shown in Figure 2.



**Figure 2.** Picture of the Hydrofloat separator used in this study.

The HF separator operates without a rotating impeller, as particle suspension is achieved by the smooth and hindered settling conditions of the particles rather than by the turbulent conditions of the traditional flotation cell. Air bubbles, generated by a novel fluidisation system, are dispersed by nozzles on an elutriation manifold. As the finely dispersed air bubbles rise through the fluidised bed, they attach to the sufficiently hydrophobic particles form particle–bubble aggregates which are sufficiently buoyant to float and be recovered. The high density of the fluidised bed eliminates axial mixing or turbulence, increases coarse particle residence time and improves the flotation rate through enhanced bubble–particle interactions, resulting in high recovery rates for both fully liberated and partially liberated particles. The up-current water velocity overcomes froth recovery restrictions, thereby promoting the recovery of coarse particles. The performance of the HF separator depends on the physical particle properties (particle density and particle size distribution), ore properties (mineralogy, liberation and texture), hydrodynamic conditions (bed height, superficial air and water flow rates, etc.) and chemical conditions (reagent types, dosages, etc.).

The HF technology has been successfully applied in the coarse flotation of industrial minerals, in which particles coarser than 3 mm can be recovered at industrial scale. Recent studies at laboratory and pilot scales have also shown that the HF can recover low-grade coarse sulphide middlings that cannot be recovered by conventional flotation machines [22–26]. Paiva and Rubio [16] demonstrated that the HF achieved higher recoveries of classified, coarse fractions of  $-297 + 210 \mu\text{m}$  and  $+297 \mu\text{m}$  than conventional flotation (CF) for a copper sulphide mineral as an example of a difficult-to-liberate ore at laboratory scale. Miller et al. [27] showed that the HF was able to recover metalliferous values at a grind size much coarser than that treated in industrial concentrators during the flotation of a low-grade gold ore. Miller et al. [27], using high-resolution X-ray microtomography (HRXMT), showed that the HF recovered nearly 100% of the 0.850–0.500 mm composite particles containing as little as 1% surface exposure of sulphide mineral in scavenging applications. They further showed that tailings contained virtually no particles containing more than 1.5% exposed sulphide grain surface area. Fosu et al. [28] concluded that the HF outperformed the CF for the upper particle size of about 500  $\mu\text{m}$  during the flotation of model synthetic composites of quartz in a lead borate matrix with simple and locking texture at laboratory scale. Awatey et al. [29] showed that the recovery of coarse sphalerite using the HF increased with increasing bed level, superficial water and gas flow rates. They also demonstrated that there exist thresholds for each operating parameter, above which recovery started to decrease. They also established that the HF outperformed the CF in the recovery of the  $+425 \mu\text{m}$  sphalerite particles. Awatey et al. [30] found that the critical contact angle required to float coarse sphalerite particles in CF was higher than in HF, and increased as particle size increased for the flotation of sphalerite (0.250–1.180 mm) at laboratory scale. The HF was found to outperform the CF at the same particle size and contact angle of the coarse sphalerite particles.

Despite being successfully commissioned in the coarse flotation of industrial minerals and sulphide middlings, HF technology has not yet been applied in platinum group minerals (PGMs) flotation. Coarse PGM ore grinding would increase energy efficiency, and avert the undesirable generation of fines and sliming of PGMs and BMS due to overgrinding. Furthermore, coarse PGM ore flotation using HF would overcome challenges associated with the recovery of fines. This study investigated the amenability of PGM-bearing ore to treatment using HF technology.

## 2. Materials and Methods

### 2.1. Sample Preparation

Platreef ore from the Bushveld complex (BC) in South Africa was investigated in this study. A 1000 kg of feed material was crushed to 100%  $-1.7 \text{ mm}$  using a cone crusher. The crushed sample was then dry-milled for 40 min, using a ball mill utilising high chrome media in 30 kg batches. After milling, all the milled samples were blended and homogenised

to prepare one composite, which was dry-screened using 106  $\mu\text{m}$  and 300  $\mu\text{m}$  sieves to produce a +106 – 300  $\mu\text{m}$  size fraction. The +106  $\mu\text{m}$  size fraction was further dry-screened to obtain +106 – 150  $\mu\text{m}$ , +150 – 212  $\mu\text{m}$ , +212 – 250  $\mu\text{m}$  and +250 – 300  $\mu\text{m}$  classified size fractions. Some 2  $\times$  500 g sub-samples were removed from each size fraction for mineralogical and chemical analysis. The –106  $\mu\text{m}$  material was removed to minimise the effect of hydraulic entrainment during HF tests. This is a common practice for coarse particle flotation (CPF) investigations.

## 2.2. Particle Size Distribution

The particle size distribution (PSD) of the +106 – 300  $\mu\text{m}$  size fraction was characterised, and the results are presented in Figure 3.

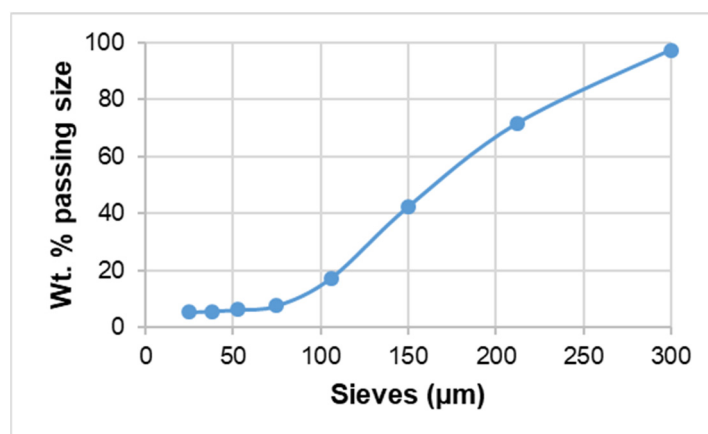


**Figure 3.** Particle size distribution of the of the +106 – 300  $\mu\text{m}$  size fraction.

The presence of the –106  $\mu\text{m}$  size fraction is due to the inefficiency associated with the dry-screening method. For the purposes of the test work, this was considered acceptable.

## 2.3. Ore Chemistry

Chemical analysis was conducted on sub-samples using fire assay methods for the 3E (Pt, Pd & Au) assays, inductively coupled plasma-optical emission spectroscopy (ICP-OES) (Thermo Fisher Scientific, Waltham, MA, USA) for base metal sulphides, and LECO for total S. The head grades of the ore presented in Table 1 show that the ore had ~2.59 g/t 3E, 0.08% Cu and 0.16% Ni. All percentages reported in the manuscript are weight percentages unless indicated otherwise.

**Table 1.** Head grades of Platreef ore.

3E	Cu	Ni	Fe	Total S
(g/t)	(%)	(%)	(%)	(%)
2.59	0.08	0.16	6.39	0.28

## 2.4. Size by Assay

A 1 kg sub-sample was removed from the milled composite sample for size by assay (SBA) determination. The sub-sample was wet-screened at 25  $\mu\text{m}$ . The screen undersize was dried and weighed, while the oversize was dried and subjected to sizing using a root two-sieve series to 300  $\mu\text{m}$ . The masses retained on each screen were weighed to determine a full-size distribution. The SBA and mass distribution data are shown in Table 2.

**Table 2.** SBA and mass distribution data of the milled composite sample.

Sieve Size ( $\mu\text{m}$ )	Mass (g)	Mass (%)	Grade			Mass Distribution (%)		
			3E (g/t)	Cu (%)	Ni (%)	3E	Cu	Ni
+300	6.72	2.3	2.59	0.063	0.10	2.9	1.3	2.1
−300 + 212	68.31	23.2	2.36	0.062	0.09	26.5	13.0	20.3
−212 + 150	81.77	27.7	1.75	0.073	0.10	23.5	18.4	25.8
−150 + 106	76.83	26.1	1.62	0.11	0.10	20.4	26.0	24.5
−106	61.07	20.7	2.67	0.22	0.14	26.8	41.3	27.3
Total	294.7	100.0				100.0	100.0	100.0

The results in Table 2 show that the 3E and BMS were deported in both the fine ( $-106 \mu\text{m}$ ) and coarse ( $+106 - 300 \mu\text{m}$ ) size fractions. It is clear that for the coarse particle size fraction, the coarser the particle, the higher the 3E grade, while an opposite trend was observed for the Cu. There was no variability in the Ni grades across the coarse particle size fraction. From a flowsheet design perspective, a split feed circuitry would be required to process the ore. The coarse size fraction would be processed using coarse particle flotation technologies such as the HF technology, while the fine size fraction ( $-106 \mu\text{m}$ ) would be processed using conventional flotation machines. The results further show that by removing the  $-106 \mu\text{m}$  particle size fraction, 73%, 59% and 73% of the 3E, Cu and Ni, respectively were retained in the coarse particle size fraction.

### 2.5. Mineralogy

Mineralogical analysis was conducted on the feed using automated scanning electron microscopy (FEI, Hillsboro, OR, USA) with a mineral liberation analyser (Quanta 650 FEG MLA), and quantitative X-ray diffraction (XRD) (Bruker, Billerica, MA, USA). PGM, BMS and gangue-specific attributes were extracted from mapped particles in the screened feed, the concentrate and tails samples, whereas QXRD determined the bulk modal mineralogy of the concentrate and tails. Bulk modal mineralogy showed that the major gangue minerals were enstatite, plagioclase, anorthite and chlorite.

### PGM Characteristics

Based on 84 intersected grains, PGE-tellurides were the dominant PGM species, reporting at  $\sim 62.1 \text{ vol}\%$  followed by PGE-sulphides, PGE-arsenides and trace amounts of PGE-alloys. Approximately  $15.9 \text{ vol}\%$  of PGMs recorded a  $0-3 \mu\text{m}$  size class,  $\sim 45.9 \text{ vol}\%$  of PGMs a  $3-6 \mu\text{m}$  size class,  $\sim 12.5 \text{ vol}\%$  of PGMs a  $6-9 \mu\text{m}$  size class, and  $\sim 25.7 \text{ vol}\%$  of PGMs a  $9-12 \mu\text{m}$  size class. The PGMs displayed poor liberation, with  $\sim 4.5 \text{ vol}\%$  of PGMs being fully liberated. Some  $31.2 \text{ vol}\%$  of the PGMs were associated with the BMS (chalcopyrite, pentlandite, pyrrhotite and pyrite). The majority of PGMs identified in the sample were associated with gangue in the form of enstatite, chlorite, diopside, magnetite, plagioclase, quartz, hornblende and mica, as shown in Figure 4.

### 2.6. Hydrofloat Tests and Procedure

A laboratory Hydrofloat cell with a diameter of 6-inches was used for the coarse flotation of the Platreef ore. The experiments were conducted in batch mode with 10 kg of the dry basis of material, pulped at 77% solid pulp density, and conditioned in an 88 L rotating drum to prepare the feed for the HF testwork. Sodium isobutyl xanthate (SIBX), a sulphide collector, was dosed at 120 g/t (unoptimised dosage) and conditioned for 2 min. The conditioned pulp was slowly fed to the HF separator using a vibrating over-head feeder, which discharged the feed material into a central feed well at the top of the HF separator. A frother, Senfroth 522, was continuously pumped at a flow rate of 3.98 L/h into the water line using a peristaltic pump. Both the SIBX and Senfroth 522 were prepared at

1% concentration. Depending on the set value of the bed height (BH), the time required to form the fluidised bed varied between 15 and 20 min. The concentrate and tailings samples were only conducted after the system had stabilised and reached a steady state. HF tests were conducted using the classified feed material (+106 – 150  $\mu\text{m}$ , +150 – 212  $\mu\text{m}$ , +212 – 250  $\mu\text{m}$  and +250 – 300  $\mu\text{m}$ ) and the unclassified size fraction (+106 – 300  $\mu\text{m}$ ).

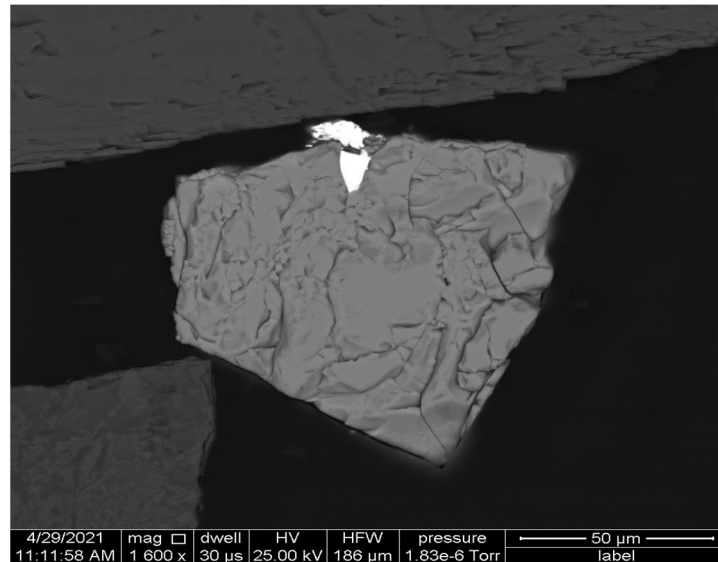


**Figure 4.** Backscattered electron image of a PGM grain attached to gangue in the feed.

Three hydrodynamic parameters, bed height (BH), air flow rate (AFR), and water flow rate (WFR), were investigated, with only one parameter being varied at a time. The BH is measured as the vertical distance between the pressure transducer mounted just above the dewatering cone and the top of the fluidised bed. The bed height is controlled using a feedback control loop linking the pressure transmitter to the underflow control valve. The AFR and WFR were read from the respective flowmeters. For the baseline test, the AFR, WFR and bed BH were set at 15 L/h, 150 L/h and 28.8 cm, respectively. The concentrate was collected into a settling tank and allowed to settle. The tailings were discharged at the end of each test. Both the concentrate and tailings samples were dried and then screened into different size fractions for chemical analysis.

### 2.7. Denver Machine Flotation Tests Procedure

A series of batch flotation tests were conducted using the +106 – 150  $\mu\text{m}$ , +150 – 212  $\mu\text{m}$ , +212 – 250  $\mu\text{m}$  and +250 – 300  $\mu\text{m}$  classified size fractions. A 1.5 kg representative sample removed from each of the size fractions was pulped at 30% solid pulp density, and then conditioned in a 2.5 L Denver flotation cell at an impeller speed of 1500 rpm. The reagent regime used for the HF tests was used for the Denver machine tests. The only exception was that the frother dosage was 50 g/t for the Denver machine tests. Flotation was conducted to extinction for both machines.

Flotation tests were conducted in duplicate for the reproducibility of mass pulls (MP), defined as a mass fraction of feed solids reporting to the concentrate. Dried concentrate samples generated from each test were blended into a bulk concentrate, and sub-samples were removed for chemical analysis using methods highlighted in Section 2.3. The same procedure was used for tailings. Chemical analysis was conducted once.

## 3. Results

This section discussed the hydrodynamic optimisation of the HF separator in the flotation of a PGM ore. The major objective of coarse particle flotation is to maximise valuable metal recovery; hence, product grades were not discussed in detail in this paper.

The flotation performances of the HF separator and the Denver flotation machine are also compared.

### 3.1. Effect of Bed Height on the HF Separator Performance

As earlier defined, the bed height is the distance between the top of the bed and the pressure transmitter. The effect of bed height on the performance of the HF separator was investigated, and the results are shown in Figure 5. Three BH values were investigated: 28.8, 32.5, and 35.0 cm. The WFR and AFR were kept constant at 150 L/h and 15 L/h, respectively.

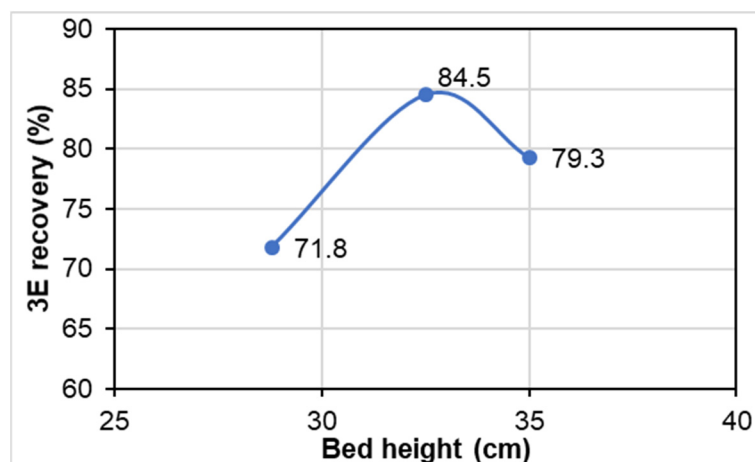
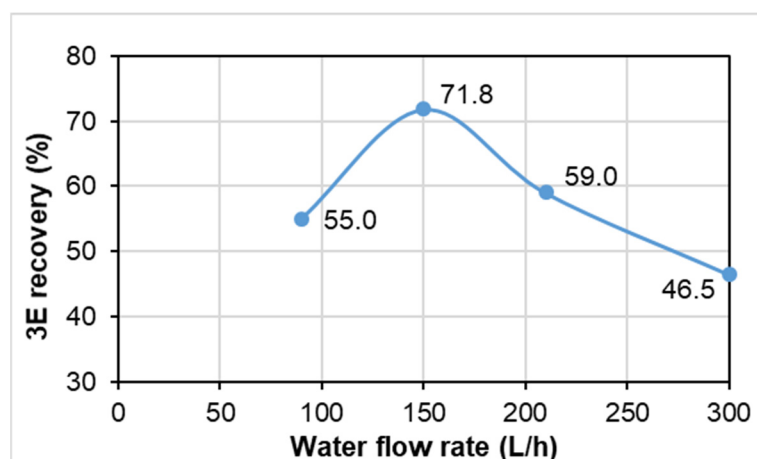


Figure 5. Effect of bed height (BH) on 3E recoveries (AFR = 15 L/h; WFR = 150 L/h).

It was observed that an increase in BH from 28.8 cm to 32.5 cm was accompanied by an increase in 3E recovery from 71.8% to 84.5% (maximum). A further increase in BH to 35.0 cm resulted in a drop in the 3E recovery to 79.3%. The 3E grades and mass pulls varied from 10.4 g/t to 12 g/t and 17.8% to 22.3%, respectively. A lower BH (i.e., a longer distance between the top of the bed and the overflow lip) may result in the detachment of the coarse and heavy particles. Settling of the coarse particles to the bottom of the separation chamber is expected at a lower BH. This explains the lower recovery at the lower BH. The increase in recovery with BH is because the travel distance of the particle–bubble aggregates at a higher BH is shorter, providing a greater chance of the coarse particles reporting to the concentrate. However, increasing the bed height above the optimum would cause turbulence, resulting in losses in valuable mineral recovery, as the results show. The sharp decrease in 3E recovery at BH values above the optimum could be due to turbulence and the splashing of the feed, as the feed well is closer to the top of the fluidised bed. This turbulence is undesirable, as it may result in the detachment of the coarse particles, thereby resulting in losses of valuable minerals. Furthermore, without turbulence, the coarse and heavy particles do have sufficient time to interact and attach to the rising bubbles, resulting in coarse particles settling on top of the fluidised bed. The results show that there exists an optimum BH at which the coarse PGMs' flotation recovery reaches a maximum, indicating that the height difference between the top of the bed and the pressure transmitter is critical. An optimum bed height of 32.5 cm was selected for subsequent test work. At this BH, the mass pull was minimum (16.5%) and the 3E recovery was maximum (84.5%).

### 3.2. Effect of Water Flow Rate

The effect of water flow rate on the performance of the HF separator was investigated, and the results are shown in Figure 6. Four water flow rates were investigated: 90, 150, 210 and 300 L/h. The BH and AFR were kept constant at 32.5 cm and 15 L/h, respectively.



**Figure 6.** Effect of water flow rate (WFR) on 3E recoveries (AFR = 15 L/h; BH = 32.5 cm).

The results in Figure 6 show that an increase in the WFR from 90 L/h to 150 L/h resulted in an increase in 3E recovery to a maximum. A further increase in the WFR to values above 150 L/h resulted in a drop in the 3E recovery. An optimum WFR of 150 L/h was therefore selected for subsequent test work. The 3E grades and mass pulls varied from 4.2 g/t to 10.4 g/t and 17.8% to 52.7%, respectively. The very high mass pull of 52.7% at 300 L/h could be a result of undesirable entrainment of gangue into the concentrate.

The HF separator is a very low-energy input device which is designed to provide a quiescent hydrodynamic environment conducive to coarse particle flotation. The rising velocity of the fluidisation water is a critical parameter influencing the performance of the HF separator. At low WFR, the rising velocity of the water is lower than the settling velocity of the coarse particles, promoting the settling of the coarse particles. Furthermore, at low WFR, the bed density is very high, such that there may be inadequate velocity to slow the settling rate of the coarse particles [29]. This may explain the observed lower 3E and BMS recoveries at the low WFR of 90 L/h. At high WFR, the rising velocity of the water is higher than the settling velocity of the coarse particles, promoting the recovery of the coarse particles, hence the observed higher 3E and BMS recoveries when the WFR was increased to 150 L/h. At very high WFR, the bed expands, and the particle–particle interaction is reduced at high WFR. This results in the bed having lower apparent viscosity and density, and thus the particles approach a free-settling condition. This condition promotes the settling of the coarse and heavy particles. Additionally, high turbulence created in the HF separator at very high WFR results in the increased particle–bubble detachment rate of coarse particles. This may explain the drop in the 3E and BMS recoveries at WFR values exceeding 150 L/h. The results demonstrate that the water rate should be increased to the optimum so that the particles can fall under hindered settling conditions. At optimum WFR, the bed density is optimal such that axial mixing or turbulence is eliminated [31]. The low turbulence favours the recovery of coarse particles by minimising the particle detachment rates [32].

### 3.3. Effect of Air Flow Rate

The effect of air flow rate on the performance of the HF separator was investigated, and the results are shown in Figure 7. Three air flow rates were investigated: 6, 15 and 24 L/h. The BH and WFR were kept constant at 32.5 cm and 150 L/h, respectively.

The results in Figure 7 show that an increase in the AFR from 6 L/h to 15 L/h resulted in an increase in 3E recovery to a maximum. A maximum PGM recovery of 71.8% was achieved at an optimum AFR of 15 L/h. A further increase in the AFR to 24 L/h resulted in a drop in the 3E recovery. The optimum WFR of 150 L/h was therefore selected for subsequent test work. 3E grades and mass pulls varied from 7.1 g/t to 12.3 g/t and 17.8% to 37.5%, respectively. The increase in the PGM recovery when the air flow rate

was increased from 6 L/h to 15 L/h could be attributed to increases in the gas hold-up and bubble size. It is generally agreed in the literature that an increase in air flow rate should also increase the number of bubbles per unit volume in the cell (gas hold-up) in a flotation cell resulting in increased particle-bubble collision frequency and bubble-particle attachment. This should result in improved metallurgical performance. Another finding in the literature is that increasing the AFR also increases the size of bubbles [33]. The increase in gas hold-up and the size of bubbles may explain the observed increase in the 3E recovery with increasing AFR. On the other hand, when AFR increases above the optimal value, a degree of turbulence is created in the HF separator, resulting in increased bubble-particle detachment. This may explain the observed decrease in the PGM and BMS recovery at high AFR values.

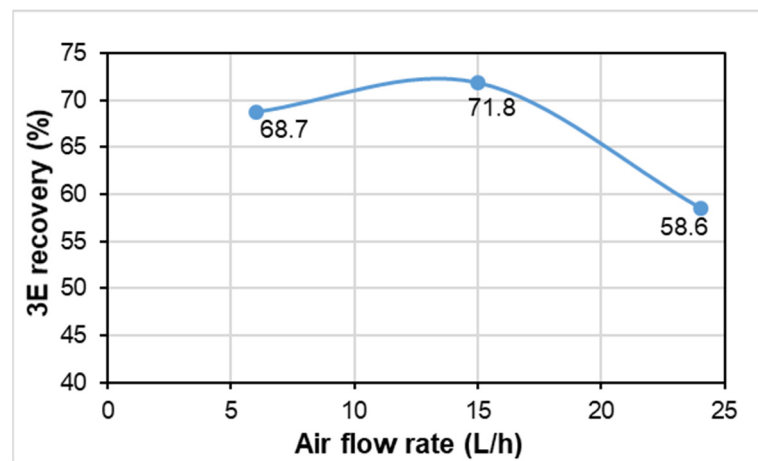


**Figure 7.** Effect of air flow rate (AFR) on 3E recoveries (WFR = 150 L/h; BH = 32.5 cm).

Overall, the results of the optimisation tests showed that an increase in the hydrodynamic parameters (BH, WFR and AFR) resulted in an increase in 3E recovery to a maximum. A further increase in the hydrodynamic parameters resulted in a decline in the 3E recovery. Similar results were observed by Awatey et al. [29], who showed that the recovery of coarse sphalerite using HF increased with the BH and WFR, and that there exists a threshold for the air flow rate, above which recovery started to decrease. However, Awatey et al. [29] concluded that the AFR had the smallest influence on the recovery of the coarse sphalerite.

For the optimised test, the results show that a reasonable 3E (Pt, Pd & Au) overall recovery of 84% was achieved at a 3E grade of 10 g/t and 16.5% mass pull, despite the PGMs being poorly liberated (4.5 vol% of PGMs being fully liberated) in the Platreef ore at a coarse grind (+106 – 300 µm). The optimised test produced a throw-away tailings grading of 0.36 g/t 3E. The results show that the HF technology has extremely low liberation requirements in the coarse flotation of the Platreef ore. The results agree with those of Miller et al. [27], who showed that the HF was able to recover metalliferous values at a grind size much coarser than that treated in industrial concentrators during the flotation of a low-grade gold ore. Miller et al. [27] showed that the HF recovered nearly 100% of the 0.850–0.500 mm composite particles with only 1% sulphide mineral surface exposure using HRXMT.

### 3.4. Recovery by Size Information for Optimised Test

Recoveries by size were characterised for the optimised HF test to assess the contribution of different narrow size classes to the overall recovery. The upgrading ratios were also characterised for the different size fractions. The recovery and upgrading ratio by size data are presented in Figures 8 and 9, respectively.

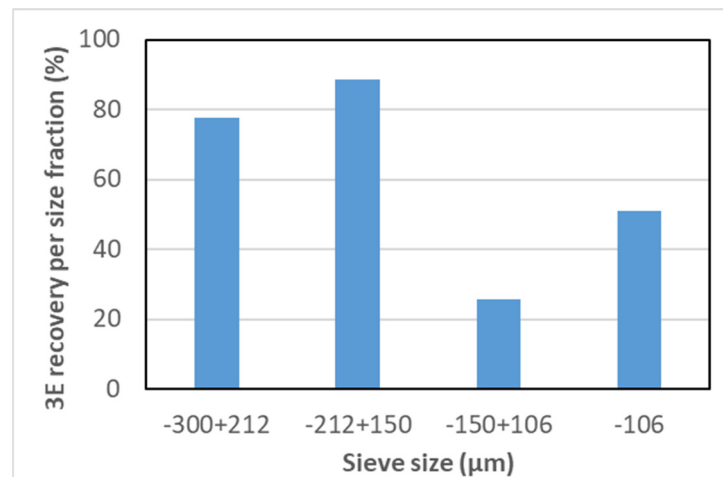


**Figure 8.** 3E recovery by size range for the different size fractions (BH = 32.5 cm; WFR = 150 L/h; AFR = 15 L/h).

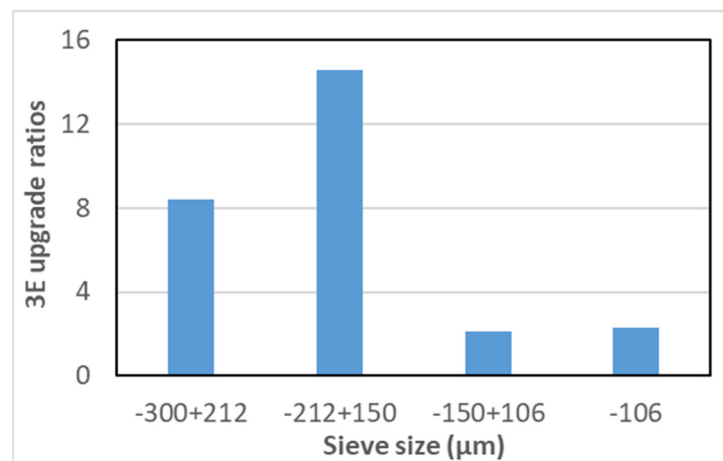


**Figure 9.** 3E upgrade ratios by size range for the different size fractions (BH = 32.5 cm; WFR = 150 L/h; AFR = 15 L/h).

Figure 8 shows that the highest 3E recovery was observed for the +150 – 212  $\mu\text{m}$ , followed by the +212 – 300  $\mu\text{m}$  particle size fractions. Figure 9 shows that the 3E upgrading ratios were higher in the coarse (+150 – 300  $\mu\text{m}$ ) size fraction than in the fine (–150  $\mu\text{m}$ ) size fraction. 3E had the highest upgrading ratio in the +150 – 212  $\mu\text{m}$  size range. The HF separator achieved a relatively lower 3E recovery and upgrading ratio for the fine (–150  $\mu\text{m}$ ) size fraction. The relatively low upgrading ratio of the fine particles could be attributed to entrainment of fine gangue, which dilutes the concentrate. The relatively lower 3E recovery in the fine size fraction could be attributed to the hydrodynamic conditions prevailing in the HF separator, which favour the recovery of coarse and not fine particles. Finer particles would require high energy input, and maybe higher collector dosages and deeper froth depth; all these conditions do not exist within the HF environment [34].

Overall, the results demonstrate that the HF achieved high recovery efficiencies and upgrading capability across the coarse size fraction (+150 – 300  $\mu\text{m}$ ). Thus, the HF separator substantially increases the upper limit of the Platreef ore, which can be successfully treated by flotation. The results suggest that the fine (–150  $\mu\text{m}$ ) size fraction should be removed from the feed to the HF separator. The implication of this finding is that a split feed circuitry which classifies the feed into two size fractions, coarse (+150  $\mu\text{m}$ ) and the fine (–150  $\mu\text{m}$ ) size fractions, is required. The coarse fraction would then be upgraded using the HF separator, while the fine size fraction would be upgraded using conventional flotation machines. This configuration maximises 3E and BMS across all the size fractions. The split

feed concept is already implemented in the processing of industrial minerals [25]. The results demonstrate that rigorous classification of the HF feed would be required to achieve high recoveries of the valuable minerals.

### 3.5. Characterisation of Flotation Products

#### 3.5.1. Concentrates and Tailings PSDs

The PSDs of the concentrates and tailings generated from the optimisation tests were characterised, and the results are presented in Figures 10 and 11.

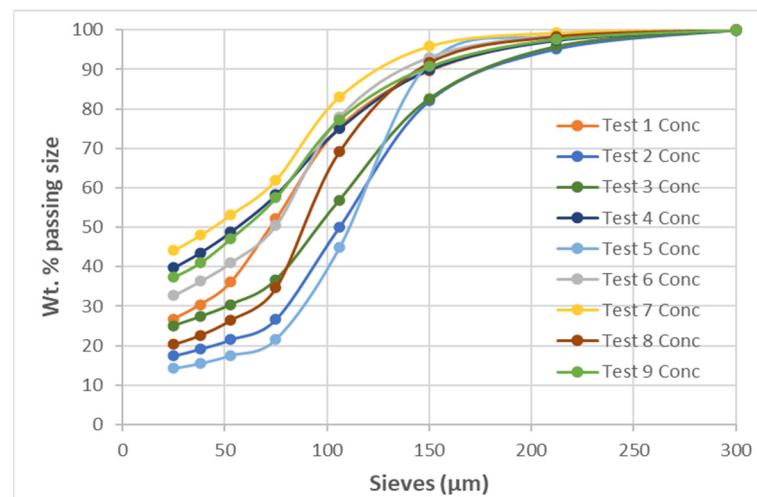


Figure 10. PSDs of all the HF tests' flotation concentrates.

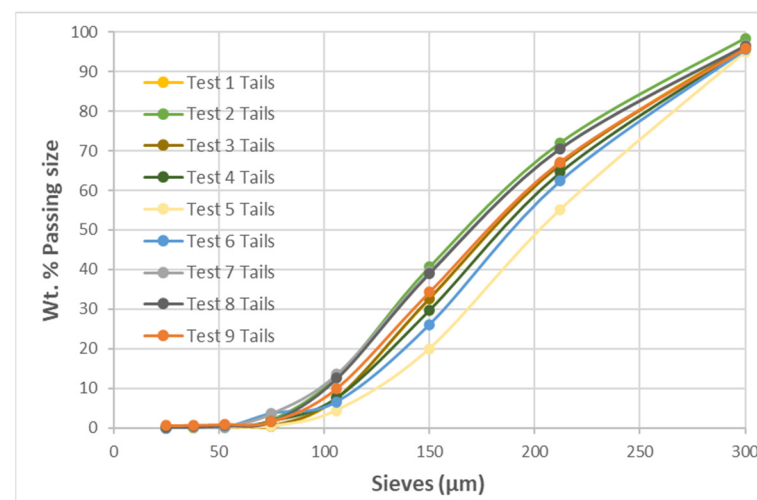


Figure 11. PSDs of all the HF tests' flotation tails.

As shown in Table 2, the feed had 2.3% of +300 µm material. The particle size distribution (PSD) of the tailings generated from the optimised test showed that it contained 4% of the +300 µm material. The PSD concentrate showed that no +300 µm material reported to the concentrate. The loss of the +300 µm material could be attributed either to sanding or to the low liberation or surface expression of the valuable minerals in the coarse particles. The results indicate that HF separator was not able to recover particles coarser than 300 microns at the conditions used. The implication of this finding is that the top size of the feed to the HF unit should be 300 µm to minimise losses in the downstream flotation circuit.

### 3.5.2. Concentrate and Tailings' Mineralogy

Mineralogical analysis was conducted on the concentrate and tailings. The mode of occurrence of the PGMs is shown in Table 3.

**Table 3.** PGM mode of occurrence in the concentrate and tailings.

Liberation Characteristic	PGM vol (%)	
	Concentrate	Tailings
Liberated PGMs	7.1	n.d.
PGMs associated with liberated BMS (base metal sulphides)	1.0	1.0
PGMs associated with BMS locked in silicate or oxide gangue particles	0.6	n.d.
PGMs attached to silicate or oxide gangue particles	2.4	9.8
PGMs associated with BMS attached to silicate or oxide gangue particles	85.2	60.7
PGMs locked within silicate or oxide gangue particles	3.7	28.6
	100	100
Number of grains	119	64

n.d. = not detected.

Mineralogical analysis in Table 3 showed that the no liberated PGMs were detected in the tailings, suggesting that the HF was able to successfully recover liberated PGMs; a higher relative abundance of liberated PGM (7.1 vol%) is found in the concentrate compared with the feed (4.5 vol%). Some 85.2 vol% of PGMs identified in the concentrate were associated with BMS attached to silicate or oxide gangue particles. The results further show that the HF separator was not able to recover most of the PGMs that were attached to or locked within silicate or oxide gangue particles. Grain size distributions (GSDs) (not presented in this paper for sake of brevity) showed that most of the PGMs in the concentrate were coarser than those in the tailings.

The BSE images of the concentrate and tailings samples illustrating mineral associations are presented in Figures 12 and 13, respectively. The BSE image in Figure 12 shows coarse liberated BMS associated with PGMs in the concentrate. Some gangue minerals associated with the valuable minerals were also recovered into the concentrate, indicating that the HF separator was able to recover some particles with very small surface expression (liberation) of the valuable minerals. The BMS (pentlandite, pyrite, pyrrhotite and chalcopyrite) detected in the concentrate were moderately to well liberated, with >70 mass% better than the 80% liberated in this sample.

The BSE image in Figure 13 shows that the majority of the coarse liberated gangue particles reported to the tailings, attesting to the good separation efficiency of the HF technology in the processing of PGM ores. Coarse gangue rejection has many advantages, including the improvement of tailings' handling, energy savings and increasing plant throughput. Some PGMs can be seen attached to gangue boundaries, while most of the PGMs were encapsulated within the gangue. The BMS (pentlandite, chalcopyrite and pyrrhotite) detected in the tailings were poorly liberated, with <55 mass% greater than 80% liberated, and were associated with gangue minerals, as shown in Figure 13. Chalcopyrite was poorly liberated, with 22.6 mass% greater than 80% liberated. The presence of the poorly liberated BMS in the tailings explains the relatively low BMS recoveries as well as the PGMs associated with the BMS. It is recommended that reagent optimisation be conducted to identify collectors that can improve the recovery of coarse, poorly liberated BMS.

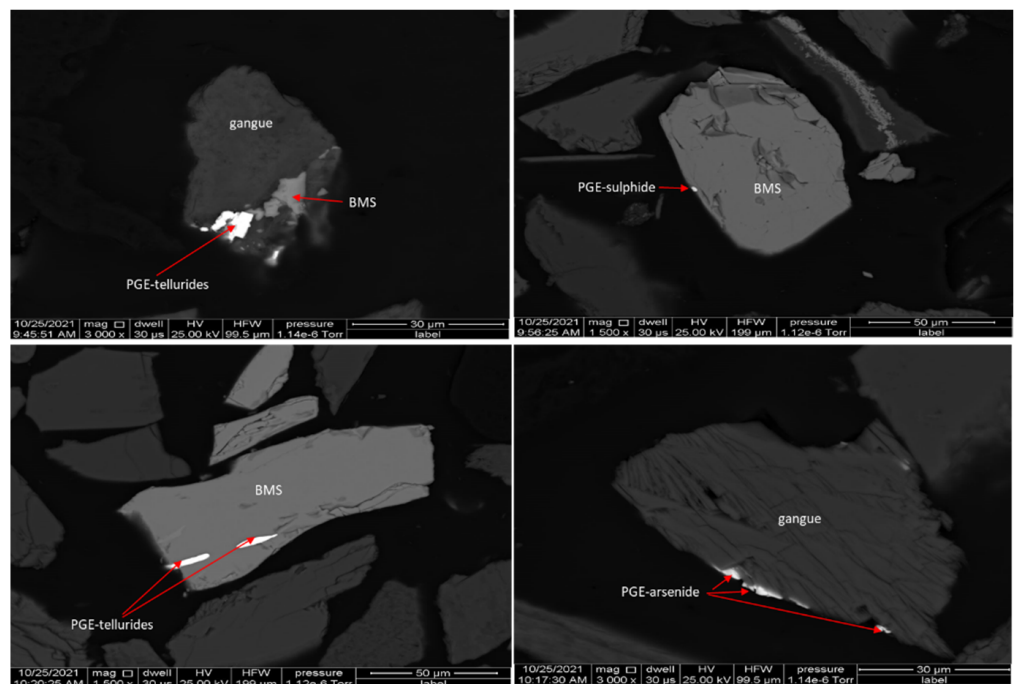


Figure 12. BSE image of the concentrate illustrating associations between gangue, BMS and PGM.

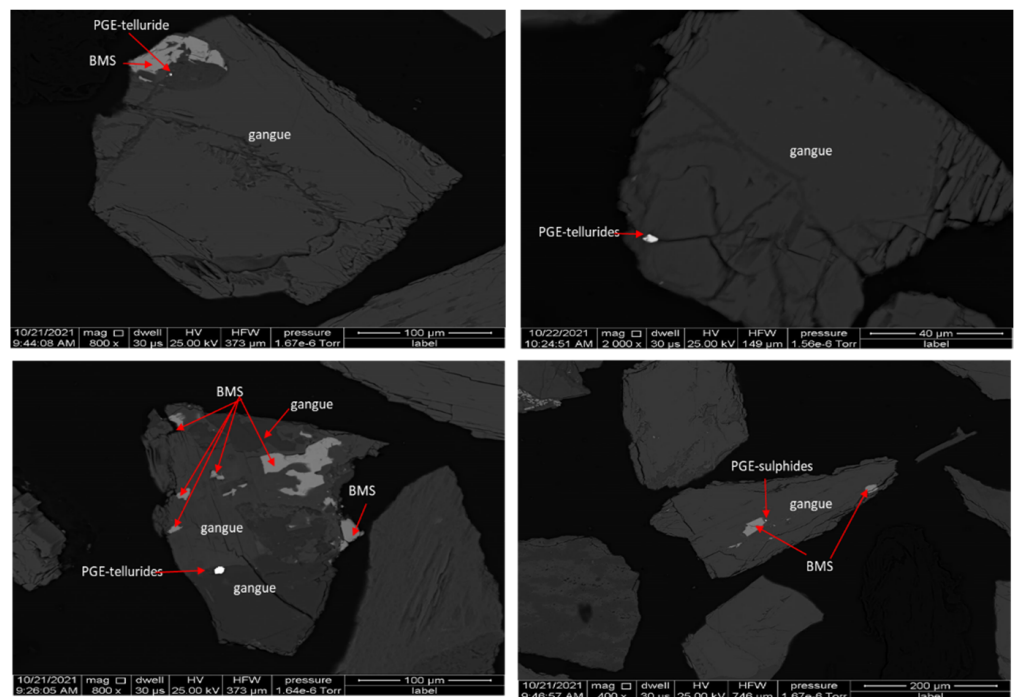


Figure 13. BSE image of the tailings illustrating associations between gangue, PGM and BMS.

Overall, the results presented in this paper suggest that the HF separator may be incorporated into existing PGM processing circuits because of its good coarse particle flotation performance. For example, the HF separator may be an attractive alternative to the mechanical cells currently used for flash flotation to recover coarse liberated PGMs and BMS in the hydrocyclone underflow stream, before recycling them back to the mill. In a mill, float, mill, float (MF2) circuit (Figure 1), the HF separator may also be used to scavenge value from the primary rougher tailings stream to recover coarse middlings prior to secondary milling. Apart from retrofitting into the existing circuits, the HF separator may also be used for pre-concentration of the ore, to reject gangue at coarse grind in novel

PGM-processing flowsheets. The novel flowsheet increases energy efficiency and plant throughput, and also reduces plant footprint.

### 3.6. Hydrofloat vs. Denver Machine CPF Performance

The coarse flotation performances of the conventional Denver machine and the HF separator were compared, and the results are presented in Figure 14 and Table 4. The reagent conditions were kept constant for both flotation machines, except for the frother, which was dosed at 3.94 L/min at 1% concentration for the HF separator, and at 50 g/t for the Denver machine. Flotation was conducted to extinction for both machines. Optimised hydrodynamic conditions of BH, WFR and AFR were used for the Hydrofloat separator tests. The following particle size distributions were investigated:  $-300 + 250 \mu\text{m}$ ;  $-250 + 212 \mu\text{m}$ ;  $-212 + 150 \mu\text{m}$  and  $-150 + 106 \mu\text{m}$ .

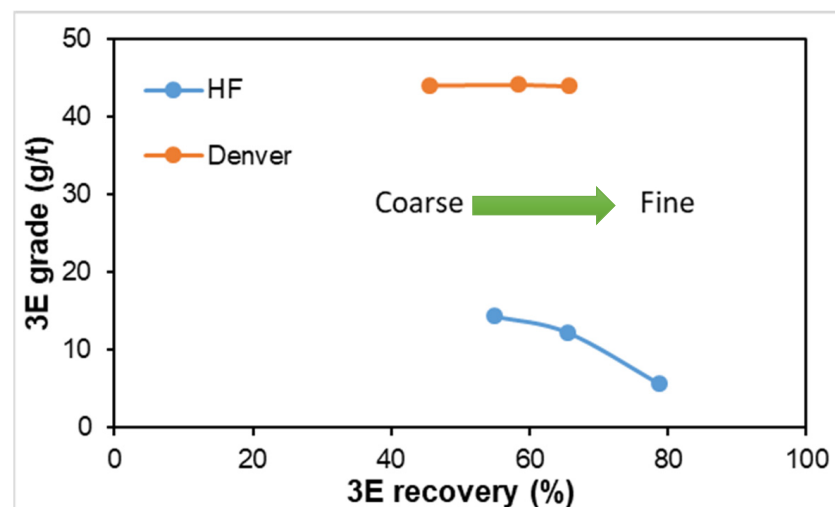


**Figure 14.** 3E grade-recovery profile for the flotation of a PGM ore using the HF separator and Denver machine.

**Table 4.** The effect of the flotation machine on 3E recovery.

Size Class ( $\mu\text{m}$ )	MP (%)		3E Recovery (%)	
	HF	DENVER	HF	DENVER
+212 – 250	7.9	1.8	55.0	45.6
+150 – 212	13.9	2.7	65.5	58.4
+106 – 150	41.1	3.4	78.8	65.7

The results show in Figure 14 and Table 4 that HF achieved higher mass pulls (MP) and 3E recoveries than the Denver machine across all size fractions. Similar results were reported by Fosu et al. [28], who concluded that the HF outperformed the CF for the upper particle size of about  $500 \mu\text{m}$  during the flotation of model synthetic composites of quartz in a lead borate matrix with simple and locking texture at laboratory scale. Similarly, Awatey et al. [29] established that the HF outperformed the CF for the recovery of the  $+425 \mu\text{m}$  sphalerite particles. Awatey et al. [29] further observed that the HF was found to outperform the CF at the same particle size and contact angle of the coarse sphalerite particles.

The extremely high mass pull of 41.1% achieved by the HF separator for the  $+106 - 150 \mu\text{m}$  could be attributed to hydraulic entrainment of the fine particles. The results also show that the Denver machine achieved higher, constant 3E grades of 44 g/t across all the size fractions. However, it should be emphasised that the major driver or key performance indicator for HF is mass pull, and consequently, recovery. The results therefore demonstrate that the HF separator outperforms the Denver machine for the

flotation of coarse particles in Platreef ore. The superior performance of HF could be attributed to the inherent design features of the HF separator. The HF separator consists of three zones, namely (i) the free settling phase, with a low solids concentration, (ii) the fluidised bed, with a plug-flow mixing regime, and (iii) the dewatering zone, with a higher percentage of solids. This design ensures low turbulence of the HF separator due to high density of the fluidised bed, which eliminates axial mixing or turbulence [31]. In this study, the HF and CF tests were conducted at 77% and 30% solid density, respectively. The low turbulence prevalent in the HF separator favours the recovery of coarse particles by minimising the particle detachment rates. The high density of the fluidised bed maximises the coarse particle residence time and enhances bubble-particle interactions, resulting in high recovery rates for both fully liberated and partially liberated particles [31]. This is because the high bed density reduces the apparent viscosity of the pulp, which reduces the rising and settling velocities of air bubbles and feed particles, respectively. The high bed density therefore provides the high particle residence time required for increased efficiency of the particle-bubble collision and particle-bubble attachment sub-processes in coarse particle flotation [32]. The bubble generator of the HF produces macro-bubbles, which improve the sub-processes. Furthermore, the percolation of the macro-bubbles through the fluidised bed may produce micro-bubbles, which attach and render the valuable minerals hydrophobic and floatable [35–37]. On the other hand, the Denver machine is characterised by high turbulence (rotor speed of 1500 rpm was selected in this study), thereby promoting the detachment of coarse particles, leading to lower recoveries [38–42].

The other reason for the higher recovery in the HF separator is that the HF separator overcomes the froth buoyancy restriction of the less buoyant coarse particles created by the froth phase in the Denver machine [29]. The HF separator operates with no/minimal overflowing froth layer due to the rising velocity of the fluidisation water. On the contrary, the Denver cell operates with a froth layer, which makes the transport of the less buoyant coarse particles from the pulp to froth phase difficult.

It is interesting to note that the 3E recoveries decreased with increasing particle size for both flotation machines. In addition to cell hydrodynamics, the differences observed in recoveries could also be attributed to mineral surface chemistry and hydrophobicity, as reported by other researchers. This suggests that multiple factors can contribute to the variations in flotation performance, and highlights the importance of a comprehensive understanding of the underlying mechanisms involved [43–47]. Awatey et al. [30] found that the critical contact angle required to float coarse sphalerite particles in CF was higher than in HF, and it increased as particle size increased for the flotation of sphalerite (0.250–1.180 mm) at laboratory scale.

#### 4. Conclusions

This study investigated the amenability of Platreef ore to coarse particle flotation using Hydrofloat™ technology. Extensive flotation testing was conducted to optimise the hydrodynamic parameters, i.e., bed height, air and water flow rates, in the flotation of coarse Platreef ore feed using the HF separator.

The results showed that Platreef ore is amenable to coarse particle flotation using the Hydrofloat™ technology. The results showed that the liberation of the valuable and gangue minerals is an important parameter affecting the recovery and separation efficiency. A reasonable 3E (Pt, Pd and Au) recovery of 84% was achieved at a 3E grade of 10 g/t and mass pull of 16%. The PGMs in the Platreef ore were poorly liberated, with 4.5% of the PGMs fully liberated at a coarse particle size range of +106 – 300 µm. The recovery by size demonstrated that the HF separator achieved high recovery efficiencies of PGMs across the 150–300 microns size fraction, and relatively lower recoveries for the sub 150 µm. The HF was therefore able to substantially increase the upper particle size that can be successfully

treated by flotation in PGM operations. Mineralogical analysis suggests that the liberated PGMs were successfully recovered in the concentrate, as there were no liberated PGMs encountered in the tailings. Composite particles of gangue, PGM and BMS were well recovered in the concentrate, although such particles also prevailed in the tailings. Most of the PGMs attached to or locked within silicate or oxide gangue reported to the tailings. It is recommended that reagent optimisation test work be conducted to identify the collector chemistry that improves the recovery of coarse, poorly liberated sulphide particles. The optimum bed level, water and air flow rates were established. An increase in bed height, water rate and air flow rate resulted in an increase in PGMs' recovery to a maximum. A further increase in the hydrodynamic parameters resulted in a decline in the PGMs' recovery. The HF separator outperformed the conventional Denver flotation machine across the following size fractions: +106 – 150 µm, +150 – 212 µm, +212 – 250 µm and +250 – 300 µm.

**Author Contributions:** Conceptualization; methodology; validation; formal analysis, J.T. and M.S.; investigation; resources; data curation; writing—original draft preparation; writing—review and editing; visualization; J.T., M.S., V.G. and D.C. All authors have read and agreed to the published version of the manuscript.

**Funding:** This research received no external funding.

**Data Availability Statement:** The data presented in this study are available on request from the corresponding author.

**Acknowledgments:** The authors wish to acknowledge the financial and technical support of Mintek, and their approval to publish the results.

**Conflicts of Interest:** The authors declare no conflict of interest.

## References

1. Schouwstra, R.; Kinloch, E.; Lee, A. A short geological review of the Bushveld Complex. *Platin. Met. Rev.* **2010**, *44*, 33.
2. Von Gruenenwaldt, G. The mineral resources of the Bushveld Complex. *Miner. Sci. Eng.* **1977**, *9*, 83–96.
3. Mwale, A.H.; Musonge, P.; Fraser, D.D. The influence of particle size on energy consumption and water recovery in comminution and dewatering systems. *Miner. Eng.* **2005**, *18*, 915–926. [[CrossRef](#)]
4. Zhu, G.; Peng, Y.; Li, Z.; Liu, C.; Li, H. Mechanism of particle size on flotation of PGMs in a fluidised bed flotation column. *Miner. Eng.* **2020**, *151*, 106338.
5. Safari, M.; Harris, M.; Deglon, D. The effect of energy input on the flotation of a platinum ore in a pilot-scale oscillating grid flotation cell. *Miner. Eng.* **2017**, *110*, 69–74. [[CrossRef](#)]
6. Hassanzadeh, A.; Safari, M.; Khoshdast, H.; Güner, M.; Hoang, D.; Sambrook, T.; Kowalczyk, P.B. Introducing key advantages of intensified flotation cells over conventionally used mechanical and column cells. *Physicochem. Probl. Miner. Process.* **2022**, *58*, 155101. [[CrossRef](#)]
7. Chanturia, V.A.; Ivanova, T.A.; Getman, V.V.; Koporulina, E.V. Methods of minerals modification by the micro- and nanoparticles of gold and platinum for the evaluation of the collectors selectivity at the flotation processing of noble metals from the fine ingraind ores. *Miner. Process. Extr. Metall. Rev.* **2015**, *36*, 288–304. [[CrossRef](#)]
8. Safari, M.; Harris, M.; Deglon, D. The effect of energy input on the flotation kinetics of galena in an oscillating grid flotation cell. In Proceedings of the XXVII International Mineral Processing Congress, Santiago, Chile, 20–24 October 2014; Volume 27.
9. Farrokhpay, S.; Filippov, L.; Fornasiero, D. Flotation of fine particles: A review. *Miner. Process. Extr. Metall. Rev.* **2021**, *42*, 473–483. [[CrossRef](#)]
10. Jameson, G.J. New directions in flotation machine design. *Miner. Eng.* **2010**, *23*, 835–841. [[CrossRef](#)]
11. Lynch, A.J.; Johnson, N.W.; Manlapig, E.V.; Thorne, C.G. *Mineral and Coal Flotation Circuits: Their Simulation and Control*; Elsevier Publishing: Amsterdam, The Netherlands, 1981; p. 291.
12. Schulze, H.J. New theoretical and experimental investigations on stability of bubble/particle aggregates in flotation: A theory on the upper particle size of floatability. *Int. J. Miner. Process.* **1977**, *4*, 241–258. [[CrossRef](#)]
13. Testa, F.G.; Safari, M.; Deglon, D.; Leal, L.d.S. Influence of agitation intensity on flotation rate of apatite particles. *REM-Int. Eng. J.* **2017**, *70*, 491–495. [[CrossRef](#)]
14. Sahu, P.; Jena, M.S.; Mandre, N.R.; Venugopal, R. Platinum group elements mineralogy, beneficiation, and extraction practices—An overview. *Miner. Process. Extr. Metall. Rev.* **2021**, *42*, 521–534. [[CrossRef](#)]
15. Hoseinian, F.S.; Rezai, B.; Safari, M.; Deglon, D.; Kowsari, E. Effect of hydrodynamic parameters on nickel removal rate from wastewater by ion flotation. *J. Environ. Manag.* **2019**, *244*, 408–414. [[CrossRef](#)]

16. Paiva, M.; Rubio, J. Factors affecting the floto-elutriation process efficiency of a copper sulphide mineral. *Miner. Eng.* **2016**, *86*, 59–65. [[CrossRef](#)]
17. Hoseinian, F.S.; Rezai, B.; Safari, M.; Deglon, D.; Kowsari, E. Separation of nickel and zinc from aqueous solution using triethylenetetramine. *Hydrometallurgy* **2021**, *202*, 105609. [[CrossRef](#)]
18. Safari, M.; Deglon, D. Evaluation of an Attachment–Detachment Kinetic Model for Flotation. *Minerals* **2020**, *10*, 978. [[CrossRef](#)]
19. Jameson, G.J.; Nguyen, A.V.; Seher, A. The flotation of fine and coarse particles. In *Froth Flotation—A Century of Innovation*; Fuerstenau, N., Jameson, G., Yoon, R.-H., Eds.; SME: Littleton, CO, USA, 2007; pp. 339–372.
20. Safari, M.; Hoseinian, F.; Deglon, D.; Filho, L.L.; Pinto, T.S. Investigation of the reverse flotation of iron ore in three different flotation cells: Mechanical, oscillating grid and pneumatic. *Miner. Eng.* **2020**, *150*, 106283. [[CrossRef](#)]
21. Trahar, W.J.; Warren, L.J. The floatability of very fine particles—A review. *Int. J. Miner. Process.* **1976**, *3*, 103–131. [[CrossRef](#)]
22. Safari, M.; Deglon, D. An attachment-detachment kinetic model for the effect of energy input on flotation. *Miner. Eng.* **2018**, *117*, 8–13. [[CrossRef](#)]
23. Rinne, A.; Peltola, A. On lifetime costs of flotation operations. *Miner. Eng.* **2008**, *21*, 846–850. [[CrossRef](#)]
24. Kohmuench, J.N.; Thanasekaran, H.; Seaman, B. Advances in coarse particle flotation: Copper and gold. In Proceedings of the AusIMM MetPlant Conference, Perth, Australia, 14–17 July 2013; p. 11.
25. Mankosa, M.J.; Kohmuench, J.N.; Christodoulou, L.; Luttrell, G.H. Recovery of values from a porphyry copper tailings stream. In Proceedings of the XXVIII International Mineral Processing Congress, Québec City, QC, Canada, 11–15 September 2016; p. 457.
26. Carelse, C.; Manuel, M.; Chetty, D.; Taguta, J.; Safari, M.; Youlton, K. The flotation behaviour of liberated Platinum Group minerals in Platreef ore under reduced reagent conditions. *Miner. Eng.* **2022**, *190*, 107913. [[CrossRef](#)]
27. Miller, J.D.; Lin, C.L.; Wang, Y.; Mankosa, M.J.; Kohmuench, J.N.; Luttrell, G.H. Significance of exposed grain surface area in coarse particle flotation of low-grade gold ore with the Hydrofloat™ technology. In Proceedings of the XXVIII International Mineral Processing Congress, Quebec City, QC, Canada, 11–15 September 2016.
28. Fosu, S.; Awatey, B.; Skinner, W.; Zanin, M. Flotation of coarse composite particles in mechanical cell vs. the fluidised-bed separator (The HydroFloat™). *Miner. Eng.* **2015**, *77*, 137–149. [[CrossRef](#)]
29. Awatey, B.; Thanasekaran, H.; Kohmuench, J.; Skinner, W.; Zanin, M. Optimization of operating parameters for coarse sphalerite flotation in the HydroFloat™ fluidised-bed separator. *Miner. Eng.* **2013**, *50–51*, 99–105. [[CrossRef](#)]
30. Awatey, B.; Thanasekaran, H.; Kohmuench, J.N.; Skinner, W.; Zanin, M. Critical contact angle for coarse sphalerite flotation in a fluidised-bed separator vs. a mechanically agitated cell. *Miner. Eng.* **2014**, *60*, 51–59. [[CrossRef](#)]
31. Tariqul Islam, M.D.; Nguyen, A.N. A numerical study with experimental validation of liquid-assisted fluidisation of particle suspensions in a HydroFloat cell. *Miner. Eng.* **2019**, *134*, 176–192. [[CrossRef](#)]
32. Xu, D.; Ametov, I.; Grano, S.R. A study of detachment of coarse particles from bubbles using novel electro-acoustical technique. In Proceedings of the CHEMECA 2009, Perth, Australia, 27–30 September 2009.
33. Gontijo, C. Coarse Particle Flotation. Ph.D. Thesis, University of South Australia, Adelaide, Australia, 2009.
34. Hassanzadeh, A.; Safari, M.; Hoang, D.H.; Khoshdast HALbijanic, B.; Kowalczyk, P.B. Technological assessments on recent developments in fine and coarse particle flotation systems. *Miner. Eng.* **2022**, *180*, 107509. [[CrossRef](#)]
35. Nazari, S.; Shafaei, S.Z.; Gharabaghi, M.; Ahmadi, R.; Shahbazi, B.; Maoming, F. Effects of nanobubble and hydrodynamic parameters on coarse quartz flotation. *Int. J. Min. Sci. Technol.* **2019**, *29*, 289–295. [[CrossRef](#)]
36. Nazari, S.; Ziaedin Shafaei, S.; Hassanzadeh, A.; Azizi, A.; Gharabaghi, M.; Ahmadi, R.; Shahbazi, B. Study of effective parameters on generating sub-micron (nano)-bubbles using hydrodynamic cavitation. *Physicochem. Probl. Miner. Process.* **2020**, *56*, 884–904. [[CrossRef](#)]
37. Fan, M.; Tao, D. A study on picobubble enhanced coarse phosphate froth flotation. *Sep. Sci. Technol.* **2008**, *43*, 1–10. [[CrossRef](#)]
38. Safari, M.; Hoseinian, F.; Deglon, D.; Leal Filho, L.; Souza, T. Impact of flotation operational parameters on the optimization of fine and coarse Itabirite iron ore beneficiation. *Powder Technol.* **2022**, *408*, 117772. [[CrossRef](#)]
39. Mohlala, M.; Ramonotsi, K.; Makhatha, M. The effect of collector dosage and particle size on coarse particle flotation of platinum group minerals in the Merensky Reef. *Miner. Eng.* **2022**, *179*, 107052.
40. Fan, Y.; Cao, B.; Guo, Y.; Liu, L. Coarse particle flotation of PGMs using a fluidised bed flotation cell with nonionic surfactant. *Miner. Eng.* **2021**, *169*, 107111.
41. Li, X.; Xia, L.; Chen, L.; Wang, C. Optimization of a fluidised bed flotation column for coarse particle flotation of low-grade sulfide ore. *Miner. Eng.* **2020**, *157*, 106518.
42. Alabi, A.O.; Dlamini, T.B.; Ndlovu, B.; Makhatha, M.M. Performance of a new type of froth flotation cell for coarse particles. *Miner. Eng.* **2020**, *151*, 106343.
43. Ma, M.; Song, S.; Ke, X.; Liu, G. Recovery of platinum group metals from low-grade sulfide ores by coarse particle flotation. *Miner. Eng.* **2021**, *163*, 106818.
44. Dube, T.; Bradshaw, D.J.; Harris, P.J. Coarse particle flotation for improving the recovery of valuable minerals in traditional flotation circuits. *Miner. Eng.* **2020**, *145*, 106115.
45. Ghorbani, Y.; Zhang, S.E.; Nwaila, G.T.; Bourdeau, J.E.; Safari, M.; Hadi Hoseinie, S.; Nwaila, P.; Ruuska, J. Dry laboratories—Mapping the required instrumentation and infrastructure for online monitoring, analysis, and characterization in the mineral industry. *Miner. Eng.* **2023**, *191*, 107971.

46. Danha, G.M.; Shengo, M.; Muzenda, E. Review on the optimisation of platinum group metal recovery through flotation. *Miner. Eng.* **2020**, *157*, 106467.
47. Zhang, K.; Song, S.; Li, Q.; Chen, L.; Zhang, L.; Zhou, J. The effect of conditioning time, collector dosage, collector type, and pH on the recovery of PGMs from a low-grade ore by flotation. *Minerals* **2019**, *9*, 368.

**Disclaimer/Publisher's Note:** The statements, opinions and data contained in all publications are solely those of the individual author(s) and contributor(s) and not of MDPI and/or the editor(s). MDPI and/or the editor(s) disclaim responsibility for any injury to people or property resulting from any ideas, methods, instructions or products referred to in the content.